The influence of silicon on the corrosion properties of FeCrAl model alloys in oxidizing environments at 600 °C

Citation for the original published paper (version of record):
Eklund, J., Jonsson, B., Persdotter, A. et al (2018). The influence of silicon on the corrosion properties of FeCrAl model alloys in oxidizing environments at 600 °C. Corrosion Science, 144: 266-276.
http://dx.doi.org/10.1016/j.corsci.2018.09.004

Corrosion Science 144 (2018) 266–276

Contents lists available at ScienceDirect

Corrosion Science

journal homepage: www.elsevier.com/locate/corsci

The influence of silicon on the corrosion properties of FeCrAl model alloys in oxidizing environments at 600 °C

J. Eklund[a,*], B. Jönsson[b], A. Persdotter[a], J. Liske[a], J.-E. Svensson[a], T. Jonsson[a]

[a] Environmental Inorganic Chemistry, Department of Chemistry and Chemical Engineering, Chalmers University of Technology, S-412 96, Göteborg, Sweden
[b] Kanthal, Box 502, 73427 Hallstahammar, Sweden

ARTICLE INFO

Keywords:
A. Alloy
A. Aluminium
B. SEM
C. High temperature corrosion

ABSTRACT

The present study investigates the influence of Si on the high temperature corrosion behaviour of FeCrAl model alloys in O_2, O_2+H_2O and O_2+H_2O + KCl at 600 °C for up to 168 h. The investigation by SEM/EDX showed that all alloys displayed a protective behaviour in dry O_2. In the more corrosive environments (O_2+H_2O and O_2+H_2O + KCl) the addition of Si affected the oxidation properties in two ways; Alloys containing Si resisted breakaway oxidation caused by Cr-evaporation (O_2+H_2O) and the thickness of the oxide formed after breakaway oxidation decreased with increasing amount of Si (O_2+H_2O + KCl).

1. Introduction

FeCrAl alloys, and the corrosion resistance of these, has been studied extensively at high temperatures (900–1300 °C) where FeCrAl alloys (about 20 wt% Cr and 1–5 wt% Al) may form a protective α-alumina. The α-alumina is reported to be the most protective alumina oxide scale giving an excellent corrosion resistance up to 1300 °C in O_2/H_2O-containing environments, see e.g. [1–3]. Due to the formation of the protective α-alumina FeCrAl alloys are commonly used as heating elements for various different applications, including the electrical elements of gas burners, furnace rollers, ignitors etc. It has been shown that FeAl alloys can form α-alumina as well but when adding chromium to the alloy, the amount of aluminium needed to form the protective layer, is decreased [4]. This is beneficial since high Al-contents have negative impacts on mechanical properties such as fabricability.

At medium high temperatures, between 700 °C and 900 °C, depending on environment and alloy composition, it is well known that the protective α-alumina layer may not form and instead transient alumina forms. The properties of the transient alumina are less known and consequently stainless steels are normally used at this temperature span as they form a protective chromia-layer [1]. However, in more corrosive environments, containing alkali salts such as KCl as well as water vapour, the protective chromia formed on stainless steels has been shown to the react with water vapour, leading to chromium evaporation [5] or alkali, leading to the formation of chromates [6–9]. Studies of the corrosion behaviour of FeCrAl alloys below 900 °C has shown that in an environment containing O_2 and H_2O, FeCrAl alloys are able to form a thin protective transient alumina layer at as low as at 600 °C [10]. The transient alumina contain small amounts of both Fe and Cr [11]. Thus, the transient alumina is less sensitive towards reaction with water vapour/alkali compared to pure chromia. However, upon introducing KCl on the sample prior to exposure, the corrosion process has been shown to drastically accelerate as a result of a rapid formation of iron-rich oxide [10]. Pre-oxidation of a FeCrAl alloy to form a thin protective alfa/transient alumina layer, prior to exposure, has shown to have a significant beneficial effect on the corrosion behaviour [12] but was sensitive towards flaws in the scale. However, a transient alumina formed on AlNi coatings has been shown to be able to resist reactions with small amounts of KCl [13]. In highly corrosive environments, the protective oxides of both alumina and chromia-formers tend to break down and form fast growing iron-rich oxide. The microstructure of this oxide has been shown to be similar for austenitic and ferritic stainless steels (FeCr and FeCrNi) as well as FeCrAl alloys at 600 °C and consists of an outward growing iron oxide as well as an inward growing spinel oxide [14–17].

Adding small amounts of specific elements may influence the corrosion properties of the alloy by increasing the protectiveness of the alumina/chromia or by altering the growth rate of the iron-rich oxide after the thin protective oxide has been lost. This is not fully understood for FeCrAl alloys in the temperature range around 600 °C.

It is well known that small amounts of alloying elements, e.g. reactive elements (RE) or Si, may strongly influence the corrosion properties of alloys. The RE effect has been studied extensively over the years and has been summarized in three extensive review articles

* Corresponding author.
E-mail address: johekl@chalmers.se (J. Eklund).

https://doi.org/10.1016/j.corsci.2018.09.004
Received 15 May 2018; Received in revised form 3 September 2018; Accepted 4 September 2018
Available online 11 September 2018

[18–20]. Studies has shown that small additions of rare earth elements, other reactive metals or stable oxide dispersions to chromia- or alumina-forming alloys have significant beneficial effects on the corrosion properties of the material. Two important effects of the addition of RE is the reduction of the scale growth rate as well as the enhanced adhesion of chromia and alumina scales [21,22]. Even though there are a large number of studies in this area, the RE effect is still not fully understood, however, there are a few hypothesis regarding the mechanisms of the effects. One suggested mechanism is that the RE may act as nucleation sites on the surface of the material, resulting in a more fine-grained initial oxide film as well as the stabilization of transient alumina phases. A suggested mechanism for the enhanced scale adhesion is the formation of "oxide pegs" extending from the oxide to the alloy substrate. In alumina forming alloys, these oxide pegs has been shown to consist of alumina which is forming by enhanced inward growth. The majority of studies regarding the effect of RE addition has been performed at higher temperatures. The influence of RE additions on the corrosion properties of stainless steels at lower temperatures (600 °C) is less studied.

Adding small amounts of silicon to stainless steels (FeCr, FeCrNi) is known to have large positive impact on the corrosion protection at high temperatures [23–25]. Continuous as well as discontinuous silica layers have been observed at high temperatures (700–900 °C). These layers may act as diffusion barriers, reducing the oxide growth rate. However, the effect of Si on FeCrAl alloys at 600 °C has not been investigated.

The aim of the present work is to study the effect of small additions of silicon on the corrosion behaviour of FeCrAl model alloys with RE at 600 °C. FeCrAl model alloys with varying silicon contents (between 0 and 2 wt% while other elements are kept fixed) have been isothermally exposed in three differently corrosive environments (Dry O_2, O_2 + H_2O and O_2 + H_2O with KCl present at 600 °C) and subsequently analysed using SEM as well as XRD.

2. Experimental procedure

2.1. Sample preparation

Three different FeCrAl model alloys were used in this study (composition of the alloys are shown in Table 1). The Cr-content in the alloys were kept low to reduce the negative effects of Cr on the mechanical properties. The alloys were first melted in a vacuum induction furnace into a 1 kg ingot. This ingot was later hot-rolled into a strip and further machined to the get a thickness of about 2 mm. The strip was also heat treated at 950 °C to achieve a more even grain size distribution. The strip was then cut into coupons with a dimension of 10 x 12 mm. A small hole with a diameter of 1.5 mm was also drilled into the sample to simplify weighing. A second heat treatment at 950 °C for one hour was performed to relax elongated grains in the bulk of the samples. However, even after the second heat treatment, the grain size varied slightly between different coupons of the same alloy. The average grain size was in the range of 110–130 µm. Prior to exposure, the sample coupons were ground to 500 grit with SiC paper and then polished down to 1 µm with a diamond suspension until a mirror-like surface had been achieved.

2.2. Exposure

Prior to exposure the samples were weighed using a Sartorius™ balance with microgram resolution. KCl was deposited onto both large surfaces of the samples by spraying a 20:80 water-ethanol solution in which KCl had been dissolved. While spraying the solution, a flow of warm air was directed towards the sample which accelerate the drying of the solution. The samples were weighed again in order to register the amount of KCl deposited on the sample. The procedure was repeated until an amount of 1 mg/cm^2 had been deposited on each sample.

The samples were exposed in a horizontal silica tube furnace in three different environments at 600 °C for 168 h. The gas flow was calibrated using a Bios Definer 220 M to achieve a total flow rate of 3 cm/s and two different gas compositions consisting of 5% O_2 + N_2(bal.) and 5% O_2 + 20% H_2O + N_2 (Bal.). In the latter gas composition, the samples were exposed both with and without KCl deposited on the surface. In the environment in which KCl was present, a short term exposure of three hours was performed for all three alloys. Samples were mounted vertically in alumina sample holders consisting of three slits in the same direction as the tube furnace. After exposure the samples were weighed again and mass gain was registered. The tube furnace set up used in this study was described by Pettersson et al. with a schematic illustration in [9].

Table 1
Nominal chemical composition (wt-%) of FeCrAl model alloys.

Alloy	Cr	Al	Si	Zr
FeCrAl**0Si**	10	4	0	0.29
FeCrAl**1Si**	10	4	1	0.29
FeCrAl**2Si**	10	4	2	0.29

2.3. Analysis

Cross sections of the samples were prepared by first gluing on a thin silicon wafer onto the surface of the sample. After the glue had dried for about 24 h they were dry cut with a low speed diamond saw and subsequently milled using broad ion beam (BIB) with a Leica TIC 3X instrument to achieve a smooth surface for more accurate analysis. The three argon guns of the BIB instrument were operated at 6.5 kV for 12 h.

The surface morphology and the cross sections of the resulting oxides of the exposed samples were analysed by means of scanning electron microscopy (SEM) (using both backscattered electrons (BSE) and secondary electrons (SE)) and energy dispersive X-ray (EDX) with an accelerating voltage of 10–20 kV using an FEI Quanta 200 equipped with an Oxford Instruments X-Max^N 80 T EDX detector. In order to closely analyse the oxide grain size on specific samples, a FEI Versa3D LoVac DualBeam FIB-SEM was used. Already prepared cross sections were polished with ions to achieve a smoother surface, making the oxide grains more distinguishable. Ion induced secondary electrons (with accelerating voltage of 30 kV and a beam current of 10 pA) were detected to achieve the image. The average oxide grain size was calculated after measuring the largest diameter of the grains in an image processing software.

Analysis with X-ray diffraction (XRD) using a Siemens Diffraktometer D5000 was also performed as a complement to the EDX-analysis to determine the crystal structure of the oxide layers of the outward growing oxide. The XRD program consisted of a locked couple scan ranging from 2θ = 0 to 80°.

3. Results

3.1. Gravimetry

3.1.1. 5% O_2 + N_2

The alloys were exposed to a dry gas mixture of oxygen with nitrogen in balance. All samples exhibit low mass gains after 168 h exposure (Fig. 1), indicating the formation of a thin protective oxide. Based on chromia/alumina the calculated thicknesses vary between 32/42(FeCrAl**2Si**) and 143/189 nm (FeCrAl**0Si**). Small differences in mass gain is observed between the samples in the zoomed in box (the right-hand corner of Fig. 1). FeCrAl**0Si** exhibits a lower mass gain than FeCrAl**1Si** while FeCrAl**2Si** shows the lowest mass gain in this environment.

3.1.2. 5% O_2 + 20% H_2O + N_2

In the O_2/H_2O-containing environment FeCrAl**0Si** exhibits a large

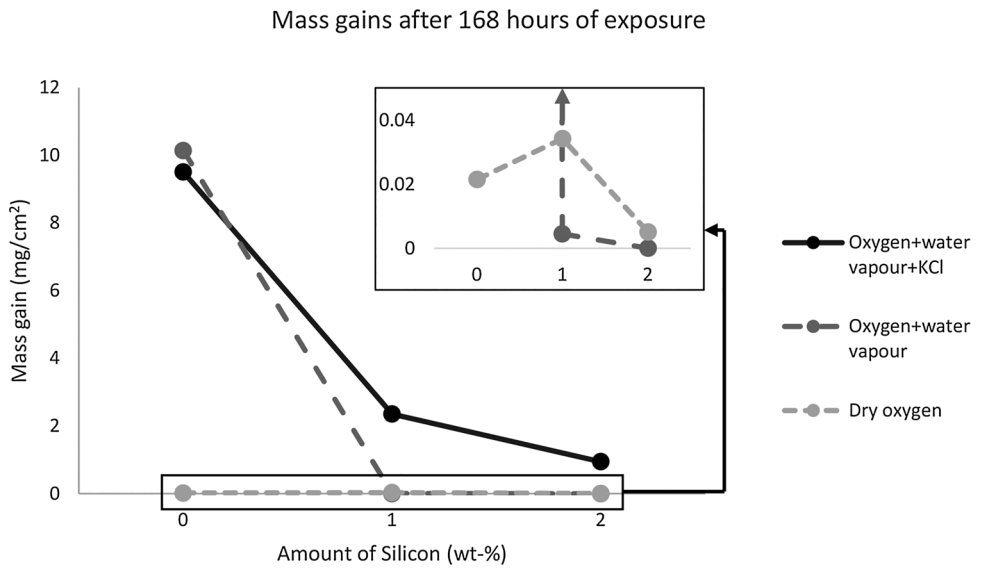

Fig. 1. Mass gains plotted against silicon content of samples exposed in 5% O_2 + 20% H_2O + N_2 (Bal.) with and without KCl present as well as 5% O_2 + N_2 (Bal.) at 600 °C after 168 h. The zoomed in box in the top-right corner shows the small differences between the low mass gain samples.

mass gain after 168 h, indicating a loss of the protective oxide leading to breakaway oxidation. However, FeCrAl**1Si** and FeCrAl**2Si** still shows low mass gains indicating the formation of a protective scale. FeCrAl**2Si** exhibits a lower mass gain compared to FeCrAl**1Si.** In the presence of water vapour FeCrAl**1Si** and FeCrAl**2Si** has a lower mass gain compared to when exposed in dry oxygen (see zoomed in box in Fig. 1)

3.1.3. 5% O_2 + 20% H_2O + N_2 + 1.0 mg/cm^2 KCl

After 168 h, the samples exposed in the environment with KCl present shows a similar trend as when being exposed to oxygen and water vapour, with a large decrease in mass gain for the silicon containing alloys (see Fig. 1). In this environment FeCrAl**1Si** and FeCrAl**2Si** exhibits higher mass gains than in the previous environments indicating breakaway oxidation, i.e. the loss of the thin protective oxide. As shown in Fig. 2, all alloys exhibit relatively high mass gains already after three hours indicating a very short incubation time to breakaway oxidation (iron oxide growth).

A gold coupon with 1 mg/cm^2 KCl was exposed in the same environment as the FeCrAl model alloys to investigate the KCl evaporation rate on a passive surface. After 24 h exposure about 70% of the KCl had evaporated from the gold surface. This means that no unreacted KCl should be left on the surface after 168 h.

3.2. Oxide morphology and microstructure

3.2.1. 5% O_2 + N_2

The surface morphology of the alloys after exposure in the dry oxygen containing environment is displayed in Fig. 3. Despite the very low mass gain the surface morphology investigation showed some regions with iron oxide on the FeCrAl0Si sample (calculated average thickness of 140 nm), see Fig. 3a. These regions represent approximately 30% of the surface and follows the alloy grain distribution, i.e. some alloy grains are covered by a thin iron oxide after 168 h exposure. Apart from this, nodules of iron oxide (of varying size) has begun to grow around individual zirconia particles. FeCrAl**1Si** has also begun to form nodules (around 20 µm in diameter) of iron oxide around

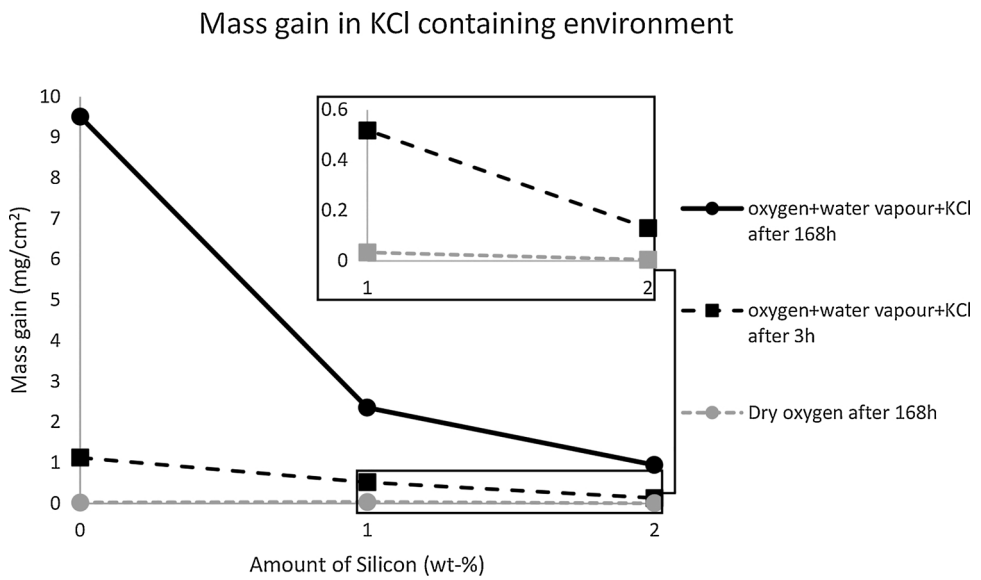

Fig. 2. Mass gains of samples exposed in 5% O_2 + 20% H_2O + N_2 (Bal.) with KCl after 3 h and 168 h. Mass gains of samples exposed in dry oxygen for 168 h are added as reference. Zoomed in box placed in top-right corner for easier comparison.

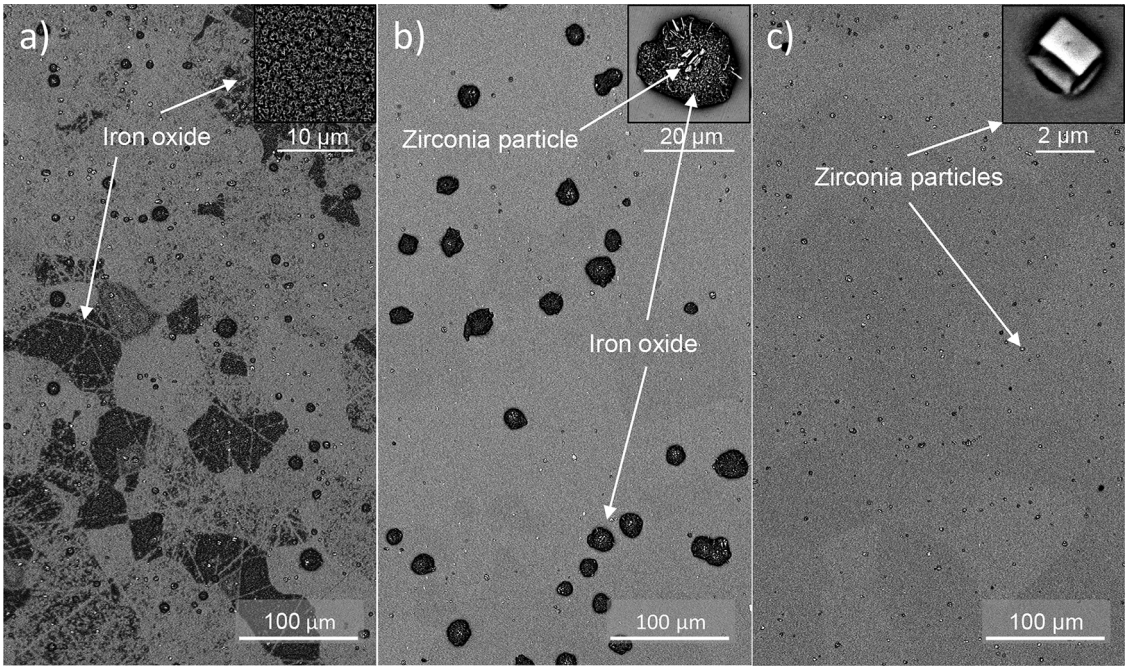

Fig. 3. SEM-BSE plan view images of a) FeCrAl**0Si**, b) FeCrAl**1Si** and c) FeCrAl**2Si** after exposure in 5% O_2 + N_2(bal.) for 168 h at 600 °C.

individual Zr particles but to a larger extent and are evenly distributed on the surface (see Fig. 3b). FeCrAl**2Si** is still showing a protective behaviour and has not yet formed any iron oxide on the surface (see Fig. 3c).

3.2.2. 5% O_2 + 20% H_2O + N_2

In Fig. 4 the surface morphology of the three alloys after exposure to the oxygen and water vapour containing environment (O_2 + H_2O) is displayed. FeCrAl**0Si** has formed a thick oxide (consisting of iron oxide confirmed with EDX analysis) and has gone through breakaway oxidation as shown by the rough surface morphology. The formation of whiskers is observed on the oxide surface (see zoomed in box in Fig. 4a). In order to investigate the thick oxide microstructure a cross-section was prepared by ion milling through the oxide into the alloy using BIB, see Fig. 5. The oxide scale is about 80 µm thick and is in good agreement with thickness calculations based on magnetite. The oxide scale consists of an outward growing iron oxide and an inward growing Fe, Cr, and Al containing oxide, indicating a spinel oxide [14,15]. The outer scale consists of an upper hematite layer (about 20 µm thick) followed by a magnetite layer (about 30 µm thick). About 4 µm into the magnetite layer there is a very porous layer (about 3 µm thick).

The inward growing spinel has formed periodic segments distinguished by dark and bright contrasts in the SEM-BSE image. EDX-analysis shows that the darker areas are richer in Al and Cr compared to

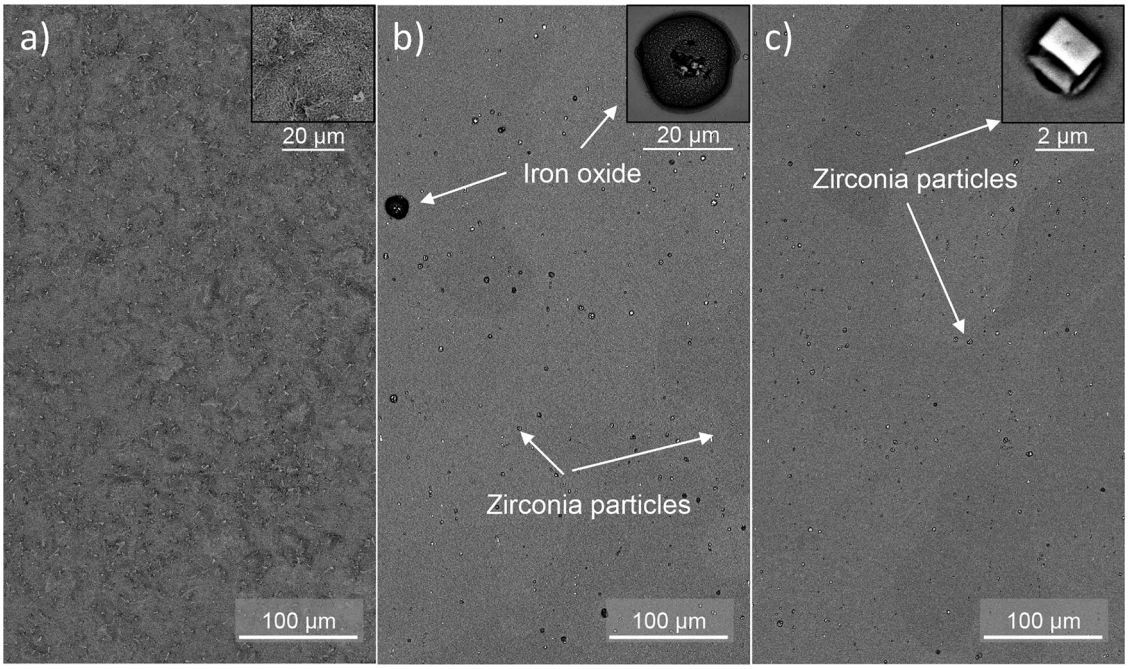

Fig. 4. SEM-BSE plan view images of a) FeCrAl**0Si**, b) FeCrAl**1Si** and c) FeCrAl**2Si** after exposure in 5% O_2 + 20% H_2O + N_2 (Bal.) without KCl present for 168 h at 600 °C.

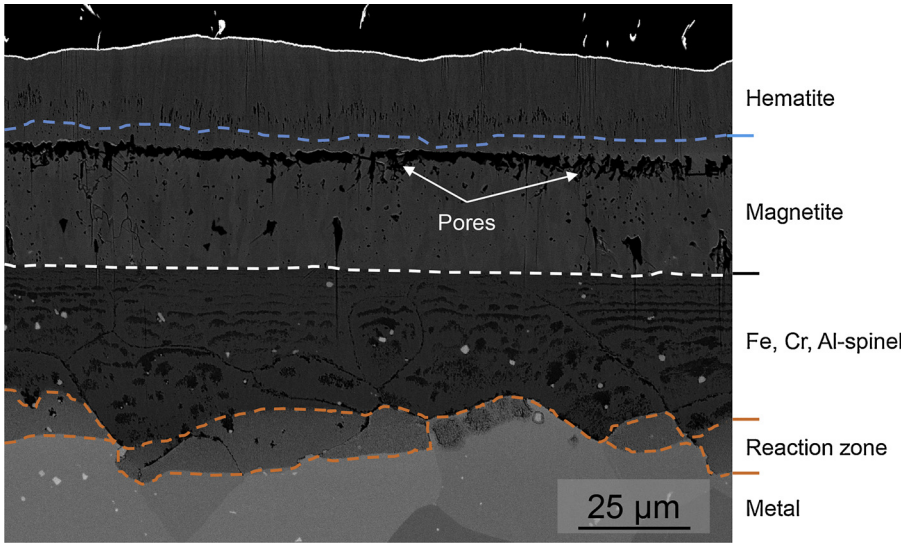

Fig. 5. SEM-BSE cross section image of FeCrAl**0Si** after exposure in 5% O_2 + 20% H_2O + N_2 (Bal.) without KCl present for 168 h at 600 °C.

the bright areas in which there is almost no Cr and about half as much Al. The same can be observed in the original alloy grain boundaries. Below the inward growing oxide there is a roughly 10 µm thick layer with brighter contrast than the oxide but darker contrast than the alloy. This is a reaction zone (also referred to as internal oxidation zone in previous studies) in which about 60% of the metal is oxidized while the remaining is non-reacted. The average amount of Al and Cr is about 40% lower in the reaction zone compared to the spinel while the Fe content is roughly 30% higher in the reaction zone compared to the spinel oxide.

FeCrAl**1Si** and FeCrAl**2Si** have formed thin protective oxides as shown by the bulk metal grains being visible through the oxide, indicating an oxide thickness in the nanometer range. FeCrAl**1Si** have formed only a few nodules of iron oxide (compared to when exposed in the dry O_2 environment). The nodules are formed around zirconia particles.

3.2.3. 5% O_2 + 20% H_2O + N_2 + 1.0 mg/cm^2 KCl

In Fig. 6 the surface morphology of the alloys after 3 and 168 h of exposure with KCl present is displayed. The rough surface morphology of all three alloys after 168 h show that none of them have retained a thin protective oxide. EDX analysis show that the thick oxide consists of iron oxide. K_2CrO_4 is detected for FeCrAl**1Si** and FeCrAl**2Si** (more for the latter) and seems to be mixed in and overgrown to by the iron oxide. Only pure iron oxide is detected on the surface of FeCrAl**0Si**. Only a small amount of unreacted KCl particles could be detected for all three alloys after 168 h of exposure. Already after three hours of exposure all three alloys have begun to form iron oxide which covers most of the surface (see zoomed in images in Fig. 6).

The SEM cross section images of the three alloys with the same magnification can be seen in Fig. 7, showing a decrease in oxide thickness with increased Si content. In Figs. 8–10, the alloys are presented in higher magnification images, in which it is possible to distinguish the different oxide layers. In Fig. 8, FeCrAl**0Si** is shown to have

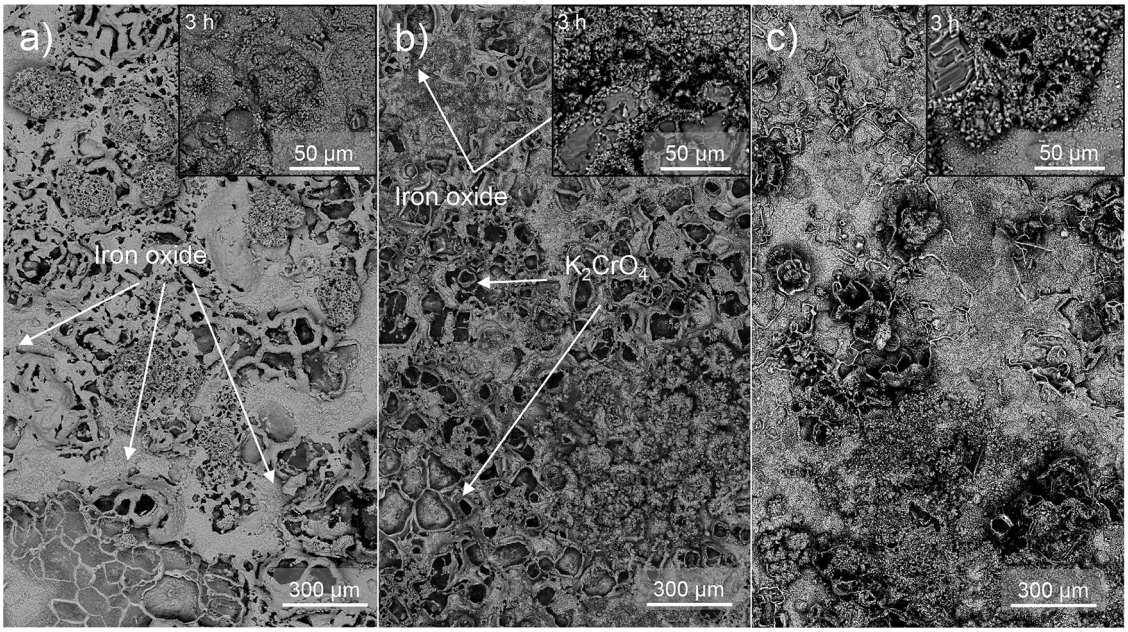

Fig. 6. SEM-BSE plan view image of a) FeCrAl**0Si**, b) FeCrAl**1Si** and c) FeCrAl**2Si** after being exposed in 5% O_2 + 20% H_2O + N_2 (Bal.) with KCl present for 168 h at 600 °C. The smaller images show the surface morphology of the alloys after 3 h of exposure.

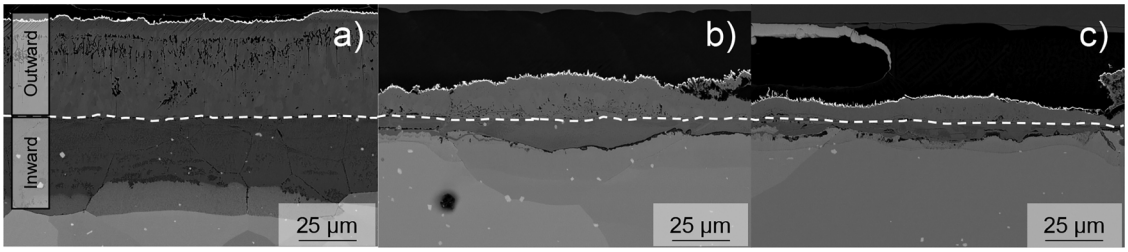

Fig. 7. SEM-BSE cross section images of a) FeCrAl**0Si**, b) FeCrAl**1Si** and c) FeCrAl**2Si** after exposure in 5% O_2 + 20% H_2O + N_2 (Bal.) with KCl present for 168 h at 600 °C.

formed a roughly 75 µm thick oxide. All three alloys have formed both an outward growing iron oxide and an inward growing Fe-Cr-Al spinel (indicated by SEM-EDX analysis and previous studies [14,15]). In FeCrAl**0Si** and FeCrAl**1Si**, the outward growing iron oxide consists of two different layers, indicated by a difference in contrast in the SEM-BSE image. The two layers are distinguished by the hatched lines in Figs. 8 and 9. From XRD analysis, it was confirmed that the outward growing iron oxide, for all of the three alloys, consisted of an upper layer of hematite and a subsequent layer of magnetite except for FeCrAl**2Si** for which a magnetite layer could not be detected. This was first indicated by the outward growing oxide only having one layer (no difference in contrast). The absence of a magnetite layer was later confirmed with XRD. The thicknesses of the different oxide layers for each alloy are presented in Table 2.

The oxide grain size is of great importance at high temperatures since this largely affects the diffusion properties in the oxide scale. Thus, the grains of the hematite and magnetite layers were made more distinguishable using a FIB-SEM (See Fig. 11) as explained in the experimental section of this article. The grain size of these layers was measured and an average was calculated for each layer (Table 3). From these measurements it is shown that the grain size of magnetite is decreasing from about 5 µm for FeCrAl**0Si** to about 3 µm for FeCrAl**1Si** while the grain size of the hematite is increasing from 163 nm for FeCrAl**0Si** to about 400 nm for FeCrAl**2Si**.

The inward growing Fe-Cr-Al spinel for the three alloys consists of areas with darker and brighter contrast. From EDX-analysis the areas with darker contrast corresponds to a slightly increased amount of Cr and Al (as well as a slight increase of Si-content in FeCrAl**1Si** and FeCrAl**2Si**). Increasing the Si content did not significantly affect the composition of the spinel apart from increasing amount of Si in the spinel. The average compositions for the different contrasts in the spinel oxide are summarized in Table 4.

Underneath the inward growing oxide of FeCrAl**0Si** there is a reaction zone, which is only 60% oxidized compared to the spinel oxide. This is not observed for FeCrAl**1Si** and FeCrAl**2Si** but instead there is a zone of nitridation, indicated by the EDX analysis. The nitridation zone seems to decrease in thickness with an increase in silicon content between FeCrAl**1Si** (around 15 µm) and FeCrAl**2Si** (around 10 µm).

4. Discussion

This aim of this study is to investigate the effect on the corrosion properties of adding small amounts of Si to FeCrAl alloys (containing small amounts of the RE Zr). This has been achieved by exposures of model alloys, with well controlled compositions to keep the amounts of all other elements fixed while Si is varied, in three differently corrosive environments.

4.1. General observations – model alloys

After the production of the model alloys, heat treatments were performed to reduce the spread in grain size. Even though some spread in grain size could still be observed after the heat treatment, repeated experiments showed good reproducibility which indicates that the scatter in grain size between the alloys is of minor importance at this temperature in these environments.

All three alloys contained small amounts of Zr. As a result of this, small Zr-rich precipitates (approximately 2 µm large) were evenly distributed in the bulk of the alloy (similar for all alloys, see Figs. 3, 4 and 7). These precipitates were in the form of Zr-nitrides in the bulk of the alloy. After exposure of the alloys, some precipitates are incorporated in the thin protective oxide (see Figs. 3 and 4) as well as in the inward growing spinel (see Figs. 8, 9) and are instead in the form of zirconia. The amount of Zr in the matrix was lower than the detection limit of the SEM/EDX in all investigated samples indicating that Zr doesn't dissolve in the matrix. It has been reported that RE additions segregates and form Re-rich particles instead of dissolving in the alloy matrix [26]. No enrichment of any of the alloying elements was observed at/in the Zr

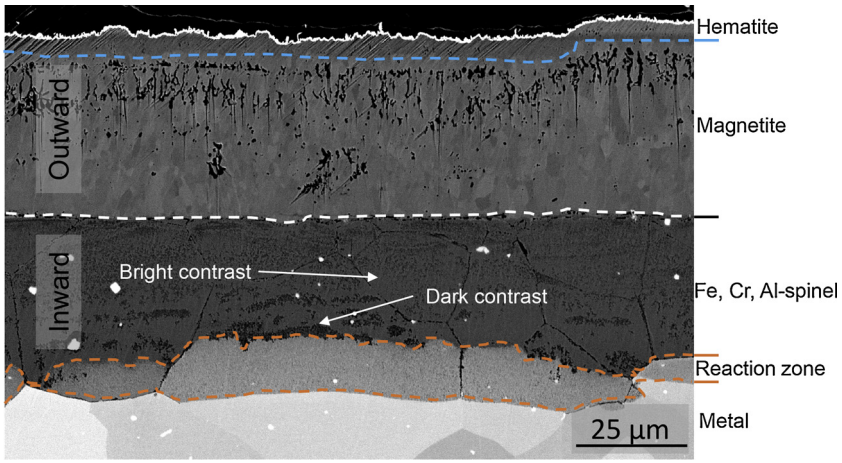

Fig. 8. SEM-BSE cross section image of FeCrAl**0Si** after exposure in 5% O_2 + 20% H_2O + N_2 (Bal.) with KCl present for 168 h at 600 °C.

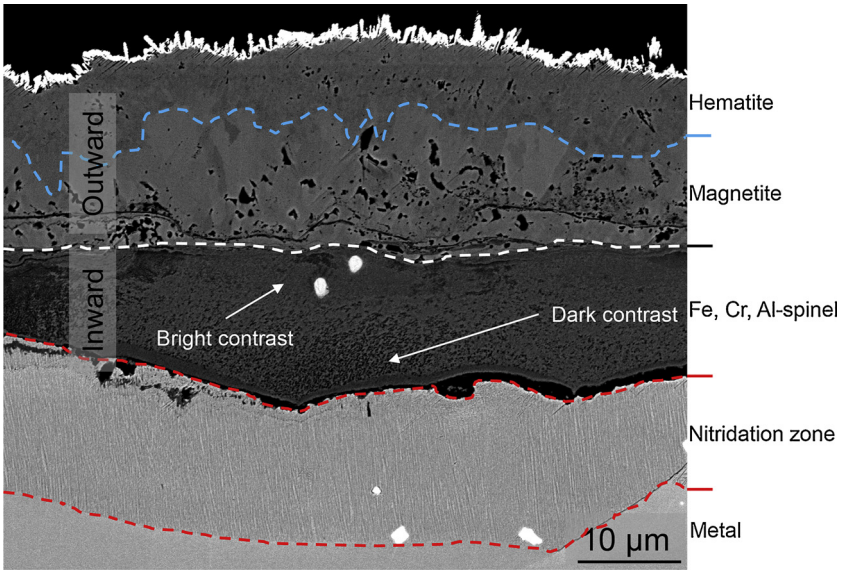

Fig. 9. SEM-BSE cross section image of FeCrAl**1Si** after exposure in 5% O_2 + 20% H_2O + N_2 (Bal.) with KCl present for 168 h at 600 °C.

rich particles.

It has been shown that iron-based chromia forming alloys experience breakaway oxidation after the breakdown of the chromia, as a result of a rapid formation of outward growing iron-rich oxide and inward growing spinel at 600 °C [14,15]. In this study, the influence of Si on both the thin protective oxides and the thick iron-rich oxides was investigated. It was shown that even after the loss of the thin protective oxide, the protectiveness of the iron-rich oxide could be influenced by changing the Si content. The oxidation is therefore defined as **primary** (thin Cr/Al rich scale) and **secondary** (thick iron rich scale) protection.

4.2. The influence of Si on the primary protection

It has been shown that conventional FeCrAl alloys (20 wt% Cr, 5 wt % Al) form a thin protective oxide scale in dry oxygen at 600 °C [10,11]. The scale formed after 168 h of exposure has been shown to be in the range of about 40 nm, consisting of a transient alumina with small amounts of both Fe and Cr according to AES analysis [11].

Accordingly, after the exposure in 5% O_2 + N_2, all three model alloys exhibited relatively low mass gains, see Fig. 1. The calculated thickness based on chromia/alumina was roughly 30/40 nm (FeCrAl**2Si**) and 140/190 nm (FeCrAl**0Si**). The difference in mass gain could be correlated to differences observed in the surface morphology, see Fig. 3. FeCrAl**0Si** formed a thin protective oxide to a large extent over the surface with some individual alloy grains covered with an iron rich oxide. This was not observed for FeCrAl**1Si** but instead formation of iron oxide nodules could be observed evenly distributed on the surface. The SEM analysis showed traces of Zr in the centre of the iron oxide nodules, indicating that the formation of these were initiated at zirconia particles. Apart from the iron oxide nodules, the surface was covered with a thin protective oxide, indicated by the mass gain and the face that the alloy grains are visible through the scale in the SEM image (see Fig. 4). FeCrAl**2Si** did not show any indications of iron oxide formation either at individual alloy grains or as nodules at zirconia particles and also had the lowest mass gain.

A thin base oxide formed all over the FeCrAl**2Si** alloy made it was possible to calculate an average thickness of the thin scale based on the mass gain of the samples. The calculated thickness based on alumina was 40 nm T. Jonsson et al. exposed a Fe-10Cr model alloy to the same conditions [16] and found that the calculated chromia thickness was 90 nm which is roughly twice as thick as the oxide scale of FeCrAl**2Si**. A more Al-rich oxide may grow slower than a Cr-rich oxide and this indicates that the protective oxide of FeCrAl**2Si** does not consist of $(Cr_x, Fe_{1-x})_2O_3$ but a $(Cr_x, Al_{1-x})_2O_3$. An aluminium rich oxide formed on a Ni_2Al_3 coating after 168 h at 600 °C in 5% O_2 + 40% H_2O + N_2(bal.) [13] showed a thickness of 30 nm, i.e. roughly in the same range as the calculated thickness for FeCrAl**2Si**. H. Josefsson et al. exposed a commercial FeCrAl alloy (Kanthal AF) in 5% O_2 + N_2 at 600 °C for 168 h which resulted in a roughly 40 nm thick oxide [11]. The composition of the oxide was analysed with AES and it was found that the oxide was

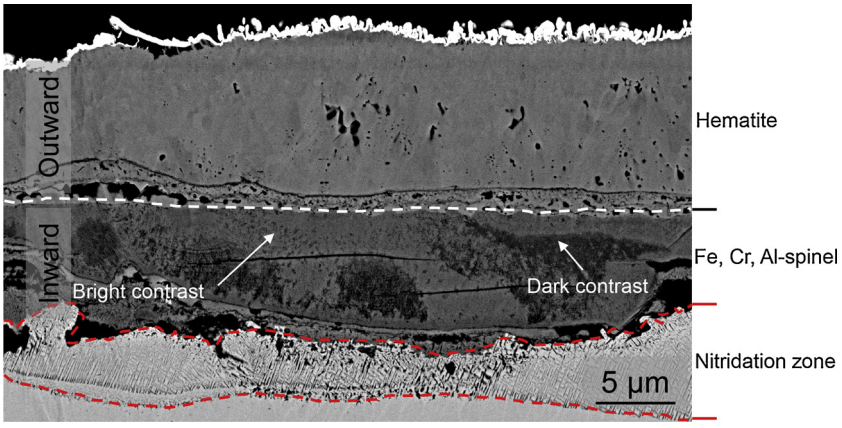

Fig. 10. SEM cross section image of FeCrAl**2Si** after exposure 5% O_2 + 20% H_2O + N_2 (Bal.) with KCl present for 168 h.

Table 2
Measured and calculated (based on magnetite) oxide thickness of FeCrAl model alloys exposed in 5% O_2 + 20% H_2O + N_2 (Bal.) with KCl present for 168 h at 600 °C.

Thickness of oxide scale (μm)					
Alloy	Total (calculated)	Total (measured)	Outward growing		Inward growing
			Hematite	Magnetite	Mixed spinel
FeCrAl**0Si**	67	67-80	5	37	25-38
FeCrAl**1Si**	17	19-32	6-8	5-9	8-15
FeCrAl**2Si**	7	8-19	5-10	0	3-9

Al-rich but also contained 6–9 at% Fe and 2–4 at% Cr. This further indicates that FeCrAl**2Si** has formed a more Al-rich oxide. In order to investigate the impact of Si on the composition of the thin scale more advanced microscopy is needed. High resolution microscopy (TEM) is ongoing in order to further investigate the composition and microstructure.

4.3. Transition from primary to secondary protection

Adding water vapour or alkali is known to accelerate the corrosion of chromia-forming steels and FeCrAl alloys at 600 °C. The vaporization of chromium(VI) oxide hydroxide has been shown to cause breakaway oxidation of Fe–Cr model alloys and commercial stainless steels in environments containing O_2 and H_2O at high temperatures, see e.g. [5]. In low oxygen activities, water vapour has in addition been shown to cause accelerated oxidation of stainless steels. However, at these conditions evaporation of chromium(VI) oxide hydroxide is negligible and various explanations has been suggested for the corrosive effect of water vapour at low oxygen activity [27–30].

Accordingly, addition of water vapour to the environment results in a drastic change in corrosion behaviour of FeCrAl**0Si** as it exhibits a high mass gain as a result of the loss of the primary protection due to reaction with water vapour, see reaction 1 [31]. This leads to a rapid formation of iron-rich oxide (secondary protection) as shown in Fig. 4 (rough surface morphology) and Fig. 5 (thick inward and outward growing oxide). The alloy without Si behaves similar to a Fe-10Cr model alloy [16] and other stainless steels at 600 °C, i.e. being vulnerable to Cr evaporation.

$$\frac{1}{2}Cr_2O_3(s) + \frac{3}{4}O_2(g) + H_2O(g) \rightleftharpoons CrO_2(OH)_2(g) \quad (1)$$

Table 3
Average grain size of magnetite and hematite for the model alloys after exposure in 5% O_2 + 20% H_2O + N_2 (Bal.) with KCl present for 168 h at 600 °C.

Grain size (μm)		
Alloy	Hematite	Magnetite
FeCrAl**0Si**	0.16	5.0
FeCrAl**1Si**	0.27	3.0
FeCrAl**2Si**	0.40	–

However, upon adding small amounts of Si (FeCrAl**1Si** and FeCrAl**2Si**) the thin protective oxide is retained as they resist the corrosive effect of the Cr-evaporation and results in both alloys with Si additions still being in the primary protection stage after 168 h of exposure in the presence of water vapour. Since the presence of water vapour is the only difference between the previously mentioned environments, these results indicate that silicon might have an effect on the supply of Cr to the oxide or the chromium evaporation induced by the water vapour. The mass gains for FeCrAl**2Si** after exposure in the O_2/H_2O-containing environment is lower than in dry oxygen as is expected when chromium evaporation still is active. Addition of Si may influence the activity of certain alloying elements in the alloys which could influence the properties of the protective scale. If the Cr activity in the alloy is increased this may result in an increased driving force to diffuse to the surface where it can react with oxygen. If so, the alloy would supply a higher amount of Cr to the surface and therefore be able to resist the breakdown of the oxide in the presence of water vapour. An increased activity of Al may on the other hand result in a more Al-rich corundum type oxide which would reduce the sensitivity towards Cr-evaporation. As shown by H. Josefsson at al [11] the oxide of a FeCrAl alloy exposed at 600 °C contains small amounts of Cr, which means that Cr-evaporation would still occur but not to the same extent compared to pure chromia. Sand et al. showed that about 0.01 mg/cm^2 of Cr evaporated when exposing an alloy that forms pure chromia in the presence of oxygen and water vapour for 90 h at 600 °C [32]. A similar exposure was performed for FeCrAl**2Si** in which an amount of 0.001 mg/cm^2 Cr had evaporated after 168 h which is much lower than for the pure chromia which indicates that the thin protective oxide is more Al-rich. The microstructural investigation showed no indications of a SiO_2 layer. However, the possible presence of a SiO_2 layer, along with the influence of Si on the composition of the thin oxides has to be further investigated with high resolution microscopy (TEM) and such a study is ongoing.

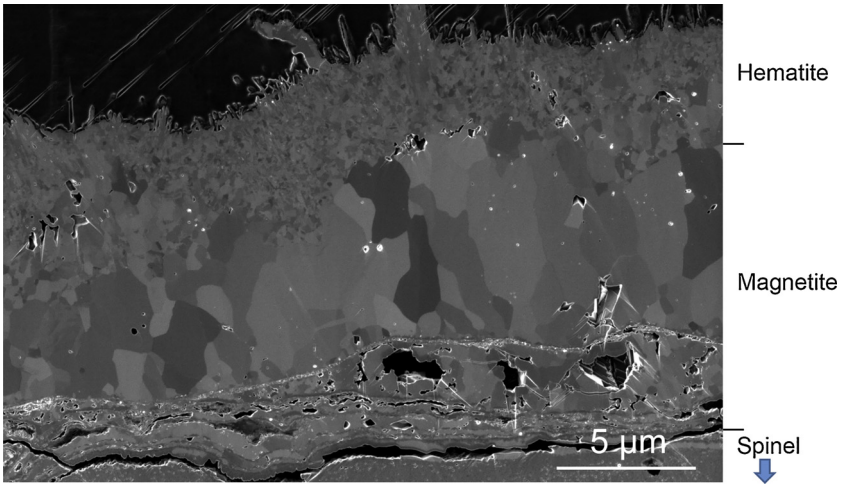

Fig. 11. Ion-induced SE cross section image of the outward growing iron oxide of FeCrAl**1Si** after exposure in 5% O_2 + 20% H_2O + N_2 (Bal.) with KCl present for 168 h.

Table 4
Chemical composition from EDX analysis at 20 kV in areas with dark and bright contrast in the spinel oxide for the model alloys. The sum of the elements equals 100% and oxygen was excluded.

Composition in dark contrast area (at-%)							Composition in bright contrast area (at-%)					
Alloy	Fe	Cr	Al	Si	K	Cl	Fe	Cr	Al	Si	K	Cl
FeCrAl0Si	52.2	24.4	22.2	0	0	1.2	60.0	20.8	19.2	0	0	0
FeCrAl1Si	37.8	28.4	26.0	6.1	0.5	1.2	55.0	21.3	19.2	4.5	0	0
FeCrAl2Si	39.5	24.7	22.2	9.8	3.0	0.8	46.1	22.2	20.3	8.7	2.3	0.4

4.4. The influence of Si on the secondary protection

The propagation mechanisms of the oxide scale formed directly after breakdown of the slow-growing $(Cr_xFe_{1-x})_2O_3$ scale of iron-based stainless steels has been described by several authors [14,15,33–37]. The oxide after breakaway was shown to consist of outward growing iron-rich oxide (hematite and magnetite) and an inward growing Fe, Cr-spinel oxide/reaction zone. The reaction zone was shown to consist of Cr-rich oxide precipitates and Cr-depleted metal.

When adding KCl on the sample surface in the environment containing 5% O_2 + 20% H_2O + N_2 it results in a rapid loss of the primary protection and a transition into the secondary protection for all three alloys. This is caused by the combination of the Cr-evaporation in the presence of water vapour (see Reaction 1) and the reaction with KCl, resulting in the formation of K_2CrO_4 and HCl (see Reaction 2 [9]). Since alumina has been shown to be relatively inert to KCl [12] the loss of the primary protection in the presence of KCl indicates that a thin Al-rich oxide does not have time to form.

$$\frac{1}{2}Cr_2O_3(s) + 2KCl(s) + H_2O(g) + \frac{3}{4}O_2(g) \rightleftharpoons K_2CrO_4(s) + 2HCl(g) \quad (2)$$

FeCrAl**0Si** forms an oxide that is roughly the same thickness as when exposed without KCl present, i.e. the presence of KCl has no additional effect on the secondary protection/growth mode, see Figs. 5 and 8. The microstructural investigation also showed that it forms a similar oxide scale in both cases. However, without KCl present, FeCrAl**0Si** forms a thicker hematite layer than with KCl present. Furthermore, Jonsson et al. exposed a Fe-10Cr alloy in 5% O_2 + 20% H_2O + N_2(bal.) at 600 °C for 168 h resulting in total oxide thickness of about 80 µm, consisting of an outward growing iron-rich oxide as well as an inward growing Fe, Cr-spinel oxide. The microstructure is very similar to that of FeCrAl**0Si** exposed in the same environment, which indicates that Al/RE does not have any influence on the corrosion behaviour without Si present [16].

The primary protection of FeCrAl**1Si** and FeCrAl**2Si** were not affected by the presence of water vapour. However, adding KCl caused a large increase in corrosivity, resulting in the loss of the primary protection and a rapid formation of iron-rich oxide, i.e. breakaway oxidation. Three hour exposures showed that all three model alloys have lost the primary protection already during the initial part of the exposure, see Fig. 6. Even though the incubation time being very short for all alloys the thickness of the formed iron-rich oxides decreases significantly upon addition of silicon. This shows that the rate of the oxide growth of the secondary protection is affected by the amount of silicon in the alloy. Even though the final oxide thickness was greatly reduced, the microstructure looks similar for the three alloys, forming both an outward growing iron-rich oxide and an inward growing spinel oxide (60:40 in ratio between outward and inward growing). However, the ratio between the hematite and magnetite differs for the different alloys. As seen in Table 2, the thickness of the magnetite layer decreases drastically upon addition of Si and results in FeCrAl**2Si** not having any magnetite but only hematite. Meanwhile, the thickness of the hematite is only varying slightly from 5 µm for FeCrAl**0Si** to a range from 5 to 10 µm for FeCrAl**2Si**. Hematite has been reported to grow slower than magnetite [39,40] and this could be a reason for the decrease in corrosion rate with increased silicon. However, the increased hematite thickness may instead be a result of the slower oxide growth rate caused by another mechanism. The grain size of hematite and magnetite also differs slightly, see Table 3, which may be of great importance since grain boundary diffusion is expected to be rate controlling at 600 °C. The grain size of hematite is increasing with Si content while the magnetite grain size is decreasing with Si content. Grain growth of magnetite has been shown at 600 °C, i.e. a slower growth rate may cause nucleation of magnetite in a later stage and thereby explain the difference in grain size.

Underneath the spinel at the metal/oxide interface of FeCrAl**0Si** there is a reaction zone (also referred to as internal oxidation zone in previous studies [27,37,41]), see Fig. 8. This could not be observed for FeCrAl**1Si** or FeCrAl**2Si** which indicates that the presence of Si may prevent internal oxidation. This could be explained by Si being prone to absorb oxygen [42] which would prevent oxygen from dissolving in the matrix and prevent the internal oxidation. If Si absorb oxygen it may result in the formation of a SiO_2 layer or dispersed SiO_2 particles. No SiO_2 layer could be observed using SEM or TEM analysis, however, dispersed SiO_2 particles may be difficult to detect even with TEM analysis. The absence of a reaction zone may improve the properties of the secondary protection by slowing down the oxide growth rate. Instead of reaction zones, FeCrAl**1Si** and FeCrAl**2Si** have both formed nitridation zones underneath the metal/oxide interface, see Figs. 9 and 10. EDX analysis indicates that these consist of precipitates of Al-nitrides. This is in good agreement with Israelsson et al [17]. Si may, as described above, prevent oxygen from dissolving in the matrix by absorbing oxygen. If oxygen is not dissolved in the matrix, nitrogen may instead dissolve which could explain the formation of a nitridation zone with Si present.

It is well known that additions of Si may result in the formation of a diffusion barrier in the form of SiO_2 at higher temperatures [23]. However, as described above, no formation of a SiO_2 layer could be observed for FeCrAl**1Si** and FeCrAl**2Si**, see Figs. 10 and 11, as well as in performed SEM-EDX analysis. This doesn't rule out the formation of a SiO_2 layer since at the temperature at which the samples were exposed in this study, the formation of SiO_2 would be very slow and may because of that be in the nanometer range [23] and therefore not visible with the SEM used. Preliminary TEM analysis indicates that no such layer has formed. Further TEM analysis is ongoing.

4.5. Comparison - Si effect of stainless steels/FeCrAl

Previous studies of stainless steels in similar environments has shown beneficial effects on the corrosion properties of small additions of silicon [43]. FeCrNi stainless steels, containing Si, has been shown to form a diffusion barrier of SiO_2 at higher temperature (900 °C) as well as at 700 °C [23]. Exposed at 900 °C in dry oxygen, the austenitic stainless steel 353 MA (Fe35Ni25Cr) was shown to form a SiO_2 layer (containing Fe, Cr and Ni) underneath a chromia layer. At this temperature, SiO_2 also began to grow into the bulk of the alloy, along the alloy grain boundaries. A SiO_2 layer also formed when exposed in the same environment but at 700 °C. The SiO_2 layer was in this case not as thick but seems to be more continuous than after the exposure at

900 °C. Also, it did not grow along any grain boundaries. However, with water vapour added, 353 MA fails to keep a thin protective chromia layer and thick iron oxide begin to grow at both temperatures but not to the same extent at 900 °C. 153 MA (Fe10Ni19Cr), which is also an austenitic stainless steel, was shown to lose the primary protection and form thick iron oxide even at 600 °C. [44]

However, it has been shown that an Fe-20Cr-20Ni alloy containing small amounts of silicon was able to form a thin SiO_2 layer after exposure for 1000 h in a CO_2 and CO_2 + H_2O containing environment at 650 °C [45]. It is however not clear if the same would occur in an environment with higher oxygen partial pressure.

Since the FeCrAl alloys used in this study are ferritic, it would be interesting to know whether silicon behaves differently in a ferritic steel compared to an austenitic steel. A ferritic Fe-20Cr alloy was exposed to the same conditions as the austenitic Fe-20Cr-20Ni alloy mentioned above [45]. It is shown that also with a ferritic stainless steel, containing small amounts of Si, a SiO_2 layer is formed which slows down the corrosion rate. The mass gain also seemed to decrease to a larger extent with increasing Si content compared to the austenitic alloys.

Studies on the silicon effect in more corrosive environments (with KCl present) are sparse. It has been shown that an Fe-15Cr alloy, modified by adding silicon, exhibited a much lower mass gain compared to the non-modified Fe-15Cr alloy when exposed at 650 °C for 48 h [46]. It was also shown that small additions of Al and Si (2.2 wt% of each) to a Fe-9Cr alloy resulted in positive synergistic effects [47]. Adding Al to the alloy resulted in an approximately 25% decrease in mass gain while adding Si to the alloy resulted in 50% decrease. However, when adding both Al and Si to the alloy it resulted in a 75% decrease in mass gain.

5. Conclusions

- In 5% O_2 + N_2, all alloys forms protective oxide scales and exhibited low mass gains. Lower Si content alloys formed small amounts of iron oxide (0 wt% Si - on alloy grains and 1 wt% Si – iron oxide nodules around Zr particles).
- In the more corrosive environments ($O_2 + H_2O$ and $O_2 + H_2O + KCl$) the addition of Si affected the oxidation properties of the model alloys in two ways:
  - In the presence of water vapour the alloys containing Si retained a thin protective oxide (primary protection) while the alloy without Si formed thick iron oxide (rapid breakaway caused by Cr-evaporation).
  - In the environment containing KCl the thickness of the iron oxide/spinel oxide, formed after breakaway, decreased with increasing amount of Si.
- The microstructural investigation showed no indications of a continuous SiO_2 layer on the Si containing alloys.

Data availability

The raw/processed data required to reproduce these findings cannot be shared at this time due to technical or time limitations.

Acknowledgements

This work was carried out within the Swedish High Temperature Corrosion Center (HTC). The authors are grateful to Kanthal for supporting and supplying materials for this study.

References

[1] P. Kofstad, High Temperature Corrosion, Elsevier Applied Science Publishers, Crown House, Linton Road, Barking, Essex IG 11 8 JU, UK, 1988.
[2] H. Götlind, F. Liu, J.E. Svensson, M. Halvarsson, L.G. Johansson, The effect of water vapor on the initial stages of oxidation of the FeCrAl alloy kanthal AF at 900 °C, Oxid Met 67 (2007) 251–266.
[3] F. Liu, H. Josefsson, J.-E. Svensson, L.-G. Johansson, M. Halvarsson, TEM investigation of the oxide scales formed on a FeCrAlRE alloy (Kanthal AF) at 900°C in dry O2 and O2 with 40% H2O, Mater. High Temp. 22 (2005) 521–526.
[4] D.J. Young, High Temperature Oxidation and Corrosion of Metals, Elsevier, 2008.
[5] H. Asteman, K. Segerdahl, J.E. Svensson, L.G. Johansson, M. Halvarsson, J.E. Tang, P. Trans tech, oxidation of stainless steel in H2O/O-2 environments - role of chromium evaporation, in: P. Steinmetz, I.G. Wright, G. Meier, A. Galerie, B. Pieraggi, R. Podor (Eds.), High Temperature Corrosion and Protection of Materials 6, Prt 1 and 2, Proceedings, Trans Tech Publications Ltd, Zurich-Uetikon, 2004, pp. 775–782.
[6] J. Pettersson, N. Folkeson, L.-G. Johansson, J.-E. Svensson, The effects of KCl, K2SO4 and K2CO3 on the high temperature corrosion of a 304-Type austenitic stainless steel, Oxid. Met. 76 (2011) 93–109.
[7] C. Pettersson, L.G. Johansson, J.E. Svensson, The influence of small amounts of KCl (s) on the initial stages of the corrosion of alloy sanicro 28 at 600 °C, Oxid. Met. 70 (2008) 241–256.
[8] S. Karlsson, J. Pettersson, L.G. Johansson, J.E. Svensson, Alkali induced high temperature corrosion of stainless steel: the influence of NaCl, KCl and CaCl2, Oxid Met 78 (2012) 83–102.
[9] J. Pettersson, H. Asteman, J.E. Svensson, L.G. Johansson, KClInduced corrosion of a 304-type austenitic stainless steel at 600°C; the role of potassium, Oxid. Met. 64 (2005) 023–041.
[10] N. Israelsson, K. Hellström, J.-E. Svensson, L.-G. Johansson, KCl-induced corrosion of the FeCrAl alloy kanthal ® AF at 600 °C and the effect of H2O, Oxid. Met. 83 (2015) 1–27.
[11] H. Josefsson, F. Liu, J.E. Svensson, M. Halvarsson, L.G. Johansson, Oxidation of FeCrAl alloys at 500–900°C in dry O2, Mater. Corros. 56 (2005) 801–805.
[12] N. Israelsson, J. Engkvist, K. Hellström, M. Halvarsson, J.-E. Svensson, L.-G. Johansson, KCl-induced corrosion of an FeCrAl alloy at 600 °C in O2 + H2O environment: the effect of pre-oxidation, Oxid. Met. 83 (2015) 29–53.
[13] K.V. Dahl, A. Slomian, T.N. Lomholt, S. Kiamehr, F.B. Grumsen, M. Montgomery, T. Jonsson, Characterization of pack cemented Ni2Al3 coating exposed to KCl(s) induced corrosion at 600 °C, Mater. High Temp. (2017) 1–8.
[14] T. Jonsson, H. Larsson, S. Karlsson, H. Hooshyar, M. Sattari, J. Liske, J.E. Svensson, L.G. Johansson, High-temperature oxidation of FeCr(Ni) alloys: the behaviour after breakaway, Oxid. Met. 87 (2017) 333–341.
[15] T. Jonsson, S. Karlsson, H. Hooshyar, M. Sattari, J. Liske, J.E. Svensson, L.G. Johansson, Oxidation after breakdown of the chromium-rich scale on stainless steels at high temperature: internal oxidation, Oxid. Met. 85 (2016) 509–536.
[16] T. Jonsson, B. Pujilaksono, H. Heidari, F. Liu, J.E. Svensson, M. Halvarsson, L.G. Johansson, Oxidation of Fe–10Cr in O2 and in O2 + H2O environment at 600°C: a microstructural investigation, Corros. Sci. 75 (2013) 326–336.
[17] N. Israelsson, K.A. Unocic, K. Hellström, T. Jonsson, M. Norell, J.E. Svensson, L.G. Johansson, A microstructural and kinetic investigation of the KCl-induced corrosion of an FeCrAl alloy at 600 °C, Oxid. Met. 84 (2015) 105–127.
[18] D.P. Whittle, J. Stringer, Improvements in high temperature oxidation resistance by additions of reactive elements or oxide dispersions, Philos. Trans. R. Soc. Lond. Ser. A, Math. Phys. Sci. 295 (1980) 309–329.
[19] B.A. Pint, Progress in Understanding the Reactive Element Effect Since the Whittle and Stringer Literature Review, (2001).
[20] D. Naumenko, B.A. Pint, W.J. Quadakkers, Current thoughts on reactive element effects in Alumina-Forming systems: in memory of john stringer, Oxid Met 86 (2016) 1–43.
[21] J.M. Francis, W.H. Whitlow, The effect of yttrium on the high temperatureoxidation resistance of some Fe-Cr base alloys in carbon dioxide, Corros. Sci. 5 (1965) 701–710.
[22] J.E. Antill, K.A. Peakall, Influence of an Alloy ADDITI on of Yttrium on the OXIDATI on Behaviour of an Austenitic and a Ferritic STA Inless Steel in CARB ON DIOXIDE, (1967).
[23] T. Jonsson, S. Canovic, F. Liu, H. Asteman, J.E. Svensson, L.G. Johansson, M. Halvarsson, Microstructural investigation of the effect of water vapour on the oxidation of alloy 353 MA in oxygen at 700 and 900°C, Mater. High Temp. 22 (2005) 231–243.
[24] S.N. Basu, G.J. Yurek, Effect of alloy grain size and silicon content on the oxidation of austenitic Fe-Cr-Ni-Mn-Si alloys in pure O2, Oxid. Met. 36 (1991) 281–315.
[25] Y. Wouters, G. Bamba, A. Galerie, M. Mermoux, J.-P. Petit, Oxygen and water vapour oxidation of 15Cr ferritic stainless steels with different silicon contents, Mater. Sci. Forum 461 (464) (2004) 839–848.
[26] D. Naumenko, W.J. Quadakkers, Reactive element additions in High temperature alloys and coatings, High Temperature Corrosion, World Scientific, 2015, pp. 245–268.
[27] E. Essuman, G.H. Meier, J. Zurek, M. Hänsel, L. Singheiser, W.J. Quadakkers, Enhanced internal oxidation as reason for breakdown of protective chromia scales on FeCr-alloys in water vapour containing gases, Materials Science Forum, Trans Tech Publ, 2008, pp. 699–706.
[28] J. Ehlers, D. Young, E. Smaardijk, A. Tyagi, H. Penkalla, L. Singheiser, W. Quadakkers, Enhanced oxidation of the 9% Cr steel P91 in water vapour containing environments, Corros. Sci. 48 (2006) 3428–3454.
[29] G. Hultquist, B. Tveten, E. Hörnlund, Hydrogen in chromium: influence on the high-temperature oxidation kinetics in H2O, oxide-growth mechanisms, and scale adherence, Oxid. Met. 54 (2000) 1–10.
[30] A. Galerie, Y. Wouters, M. Caillet, The kinetic behaviour of metals in water vapour at high temperatures: can general rules be proposed? Mater. Sci. Forum 369 (372) (2001) 231–238.
[31] H. Asteman, J.E. Svensson, L.G. Johansson, M. Norell, Indication of chromium oxide

hydroxide evaporation during oxidation of 304L at 873 K in the presence of 10% water vapor, Oxid. Met. 52 (1999) 95–111.
[32] T. Sand, C. Geers, L.-G. Johansson, J.-E. Svensson, chromium evaporation from nickel base alloy 690 in humid air at 500-900 °C, to be submitted.
[33] A.N. Hansson, K. Pantleon, F.B. Grumsen, M.A. Somers, Microstructure evolution during steam oxidation of a Nb stabilized austenitic stainless steel, Oxid Met 73 (2010) 289–309.
[34] N. Mu, K. Jung, N. Yanar, G. Meier, F. Pettit, G. Holcomb, Water vapor effects on the oxidation behavior of Fe–Cr and Ni–Cr alloys in atmospheres relevant to oxy-fuel combustion, Oxid. Met. 78 (2012) 221–237.
[35] L. Liu, Z.-G. Yang, C. Zhang, M. Ueda, K. Kawamura, T. Maruyama, Effect of water vapour on the oxidation of Fe–13Cr–5Ni martensitic alloy at 973 K, Corros. Sci. 60 (2012) 90–97.
[36] D. Young, J. Zurek, L. Singheiser, W. Quadakkers, Temperature dependence of oxide scale formation on high-Cr ferritic steels in Ar–H2–H2O, Corros. Sci. 53 (2011) 2131–2141.
[37] G.H. Meier, K. Jung, N. Mu, N.M. Yanar, F.S. Pettit, J.P. Abellán, T. Olszewski, L.N. Hierro, W.J. Quadakkers, G.R. Holcomb, Effect of alloy composition and exposure conditions on the selective oxidation behavior of ferritic Fe–Cr and Fe–Cr–X alloys, Oxid. Met. 74 (2010) 319–340.
[39] R.Y. Chen, W.Y.D. Yeun, Review of the high-temperature oxidation of Iron and carbon steels in air or oxygen, Oxid. Met. 59 (2003) 433–468.
[40] H. Larsson, T. Jonsson, R. Naraghi, Y. Gong, R.C. Reed, J. Ågren, Oxidation of iron at 600 °C – experiments and simulations, Mater. Corros. 68 (2016) 133–142.
[41] B. Pujilaksono, T. Jonsson, H. Heidari, M. Halvarsson, J.-E. Svensson, L.-G. Johansson, Oxidation of binary FeCr alloys (Fe–2.25 Cr, Fe–10Cr, Fe–18Cr and Fe–25Cr) in O 2 and in O 2+ H 2 O environment at 600 C, Oxid. Met. 75 (2011) 183–207.
[42] W. Wijaranakula, Solubility of interstitial oxygen in silicon, Appl. Phys. Lett. 59 (1991) 1185–1187.
[43] H.-h. Mao, X. Qi, J. Cao, Lc. An, Y.-t. Yang, Effect of Si on high temperature oxidation of 30Cr13 stainless steel, J. Iron Steel Res. Int. 24 (2017) 561–568.
[44] S. Kiamehr, K.V. Dahl, M. Montgomery, M.A. Somers, KCl-induced high temperature corrosion of selected commercial alloys, Mater. Corros. 67 (2016) 26–38.
[45] T.D. Nguyen, J. Zhang, D.J. Young, Effects of Silicon and water vapour on corrosion of Fe–20Cr and Fe–20Cr–20Ni alloys in CO2 at 650 °C, Oxid. Met. 87 (2017) 541–573.
[46] Y.S. Li, Y. Niu, M. Spiegel, High temperature interaction of Al/Si-modified Fe–Cr alloys with KCl, Corros. Sci. 49 (2007) 1799–1815.
[47] Y.S. Li, M. Spiegel, S. Shimada, Effect of Al/Si addition on KCl induced corrosion of 9% Cr steel, Mater. Lett. 58 (2004) 3787–3791.